

PMT Calibration and Neutron Generator Simulation for neriX

Haley Pawlow

Nevis Laboratories, Columbia University, Irvington, NY, 10533, USA

(Dated: July 31, 2014)

The nuclear and electronic recoils in Xe (neriX) experiment is designed to calibrate XENON in its search for dark matter. It precisely measures the scintillation and ionization signals resulting from incoming particles colliding in the dual-phase liquid Xenon (LXe) detector to distinguish between nuclear and electronic recoils. In the REU program, I analyzed the photomultiplier tube (PMT) calibrations by calculating the gain of the PMTs, and found that all the channels agree with the expected Poisson distribution. I also designed the neutron generator carrier by using GEANT4 to produce a Monte Carlo Simulation for neutron scattering within the carrier. In order to prevent electrical breakdown across the high voltage cable and the body of the generator, I modeled and analyzed the electric field. The final carrier design maximizes the ratio between the dielectric materials Teflon and oil.

I. INTRODUCTION

Recently, scientists have discovered that models describing everything we have been able to observe thus far on earth and the cosmos comprises about only 5% of the energy density of the universe, called normal matter. The other 95% is composed of 68% dark energy and 27% dark matter. Dark energy is the phenomenon that explains the accelerating universe. There is significant proof that dark matter exists by observing galactic rotation curves, galaxy clusters, and the cosmic microwave background. Dark matter must interact gravitationally, and through these different observations, no known matter is large enough to produce the observed gravitational effects.

In 1933, Fritz Zwicky made one of the first compelling dark matter observations. By analyzing the Coma galaxy cluster with the Virial Theorem, he calculated that its gravitational mass is much larger than expected from observations. Thus, much of that matter could be invisible or dark.[1] There has been other strong evidence from dark matter by observing galaxy clusters, namely the Bullet Cluster seen in Figure 1. The two clouds of hot x-ray gas (red) are distorted like the classic example of a shock wave produced from a bullet. This implies that there was a collision between two galaxy clusters, together forming a larger cluster. However, the blue imaging shows that there are parts of each cluster that remain undistorted, passing right through each other without any interaction aside from gravity. Gravitational lensing is defined as when light traveling from a source to the observer is bent by the curvature in spacetime of a distribution of matter between the two. The blue clouds are the apparent mass peaks from gravitational lensing, producing strong evidence for dark matter.[2]

Additionally, in 1937 Vera Rubin measured the rotational velocity of stars and gas in a spiral galaxy as a function of radius as seen in Figure 2. From there, she computed the mass of the galaxy using Newtonian mechanics

$$v(r) = \sqrt{\frac{GM(r)}{r}}. \tag{1}$$

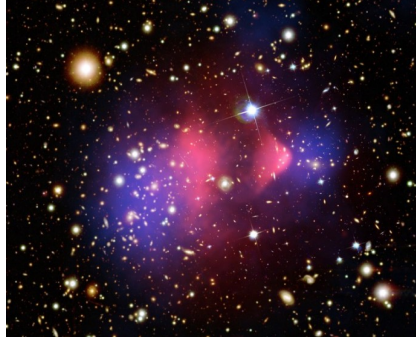


FIG. 1: The Matter of the Bullet Cluster
 X-ray: Nasa/CXC/Cfa/M.Markevitch et al.;
 Lensing Map: NASA/STScI;ESO WFI;Magellan/U.Arizona/D.Clowe et al.;
 Optical: NASA/STScI; Magellan/U.Arizona/D.Clowe et al.

Therefore, the mass should obey

$$v(r) \propto \frac{1}{\sqrt{r}} \quad (2)$$

However, the mass obeys a fairly constant velocity as seen in Figure 2.. Evidence for dark matter is also seen from gravitational lensing and the Cosmic Microwave Background (CMB).

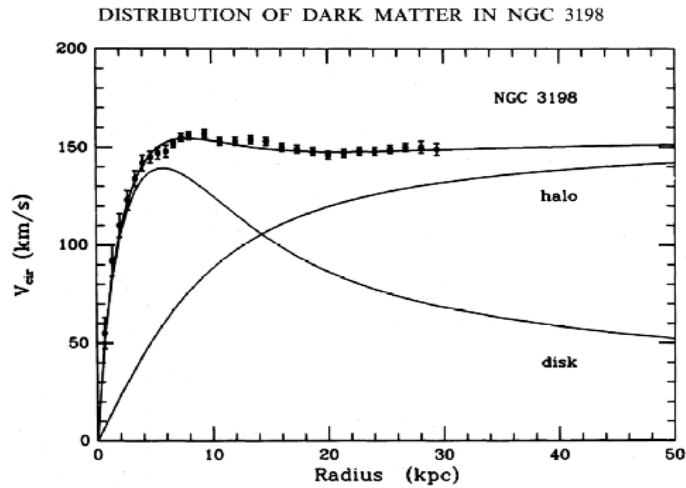


FIG. 2: Rubin discovered that in order to account for the flat-lined velocity, there needed to be an addition of matter called the dark matter halo added to the disk.

The leading candidates for dark matter are Weakly Interacting Massive Particles (WIMPs) because they agree nicely with super symmetry extensions of the standard model (SUSY). This group of particles are non-baryonic matter, charge and color neutral, non-relativistic, they interact only with the weak force, and are either stable or have lifetimes

comparable to the age of the Universe[4]. WIMPs can be detected through production of at the LHC, indirect detection that looks for particles from WIMP collisions such as positrons and gamma rays, or through direct detection which observes nuclear recoils from WIMP-nuclei collisions.

II. XENON DARK MATTER PROJECT

The XENON dark matter project uses direct detection to observe WIMPs colliding with Xe atoms and producing nuclear recoils. WIMPs can only scatter off the nuclei of atoms because they are charge neutral and only interact with the gravitational and weak force. Gamma rays, on the other hand, produce electronic recoils because they interact with the electromagnetic force. In direct detection, one can detect heat, scintillation (light), or ionization (charge). XENON detects both ionization and scintillation signals. The simultaneous measurement of two excitation channels allows XENON to discriminate between nuclear and electronic recoils. This is largely due to the fact that charged particles produce more ionization.[3].

III. NERIX EXPERIMENT

The nuclear and electronic recoils in Xe (neriX) experiment is designed to analyze how different particles, such as neutrons and gamma rays, interact with the Xe atoms. Neutrons are similar to WIMPs because they are electrically neutral and thus only collide with nuclei, thus producing nuclear recoils. It is important to calibrate XENON such that we have a clear measurement in the ratio between nuclear and electronic recoils to differentiate a WIMP from another particle. NeriX is designed to improve the nuclear and electronic recoil measurements at very low energies that have never been measured with an applied electric field (1keV).

A. Time Projection Chamber

Similarly to XENON100, neriX is also a dual-phase, noble liquid detector. In designing a direct detection experiment, one needs to pay particular attention to the material used. Xenon was chosen because of its high density of 3.10g/mL, thus enabling it to stop WIMPs within the detector. The detector is a Time Projection Chamber (TPC) as shown in Figure 3. When WIMPs collide into LXe atoms within the chamber, the atomic nuclei recoil and collide with other Xe atoms. The atoms can either be ionized, releasing electrons, or excited, emitting photons which are detected by the photomultiplier tubes (PMTs). This first signal is called the scintillation (light) signal. Then, the remaining electrons either recombine with Xe atoms or are accelerated upwards by an applied electric field across the TPC. The electrons reach terminal drift velocity quickly. Once the electrons cross over the grid to the gaseous chamber of Xe, the electrons collide with other Xe atoms. Now, the excited gas Xe atoms release photons that are detected as the ionization (charge) signal. The ability to precisely measure the scintillation and ionization signals allows neriX and XENON to distinguish between nuclear and electronic recoils.

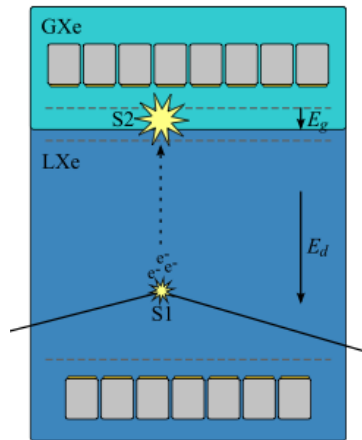


FIG. 3: Time Projection Chamber used in neriX to analyze both scintillation and ionization signals.

B. Position of event

After a recoil in LXe, electrons are accelerated across the electric field and reach a drift velocity. We can calculate the depth on an event from below the LXe surface by knowing the electric field across the chamber and the drift time between the scintillation (s1) and ionization (s2) signals as shown in Figure 4. The PMTs also record the x and y coordinates, called the hit pattern of the event. After obtaining all three coordinates, the position of the event can be reconstructed. As seen in Figure 4, the ratio between s2 and s1 is larger for electronic recoils than neutron recoils. Making precise measurements of s1 and s2 allows the distinction of WIMPs from charged particles.

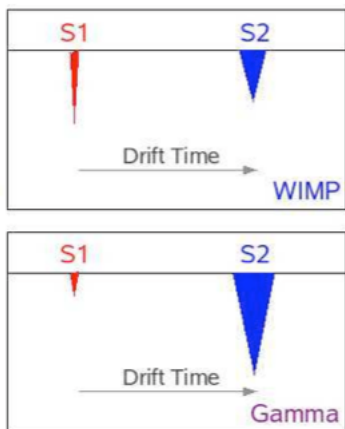


FIG. 4: The depth below the LXe surface can be calculated by knowing the precise drift time between the scintillation (s1) and ionization (s2) signals as well as the electric field applied across the chamber.

C. neriX experimental setup

In this neriX experiment we used mono-energetic neutrons that scatter in the LXe detector and deposit energy. Then, the neutrons are collected at fixed angles by two organic liquid scintillators where they deposit the rest of their energy, as seen in Figure 5. This setup allows the range of recoil energies to be chosen based on the relative position of the detectors according to the following equation

$$E_r \approx 2E_n \frac{m_n M_{Xe}}{(m_n + M_{Xe})^2} (1 - \cos\theta) \quad (3)$$

where E_n is the neutron energy, m_n is the mass of the neutron, M_{Xe} is the mass of the Xe nucleus, and θ is the scattering angle.

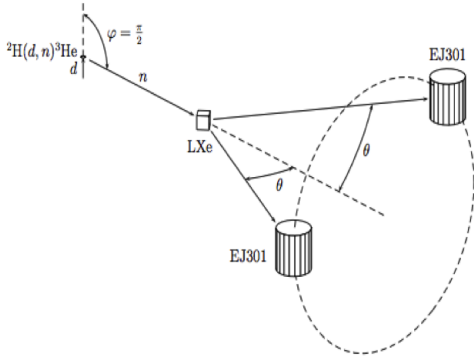


FIG. 5: The measurement principle for neriX using a neutron generator. Neutrons elastically scatter within the LXe detector, and are then detected by two organic liquid scintillators at fixed angles. [3]

IV. PROJECT 1: PMT CALIBRATION

A. PMT Design

In order to measure the scintillation and ionization signals, we need to calibrate the PMTs and analyze their gain. Shown in Figure 6, a PMT works by detecting photons. The incident photon hits the photocathode and emits a single photoelectron through the photoelectric effect. Then, the photoelectron is attracted to the first dynode by an applied electric field. Once the photoelectron accelerates from the dynode, more electrons are released which are all attracted to the next dynode. The chain of dynodes multiplies the amount of charge following a Poisson distribution, and thus producing a Gaussian distribution. The gain is defined as the number of electrons produced for one emitted photoelectron, the factor of amplification of the dynode chain.[5] The PMTs produce a gain depending on the voltage

applied to the dynode chain.

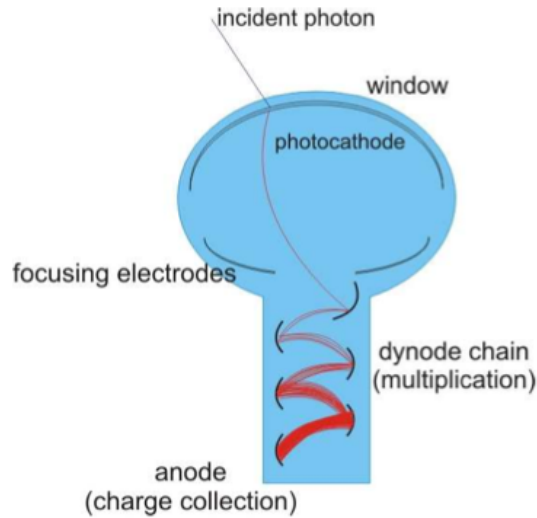


FIG. 6: Photomultiplier tubes (PMTs) convert detected photons into a measurable current signal. [5]

B. PMT Gain

The PMTs measure current which is then converted to voltage. Using Poisson statistics, we set up the PMTs such that there is noise 90% of the time, and one photoelectron 10% of the time. This guarantees that the 10% of the time we do see a signal, it is due to only one photoelectron. Figure 7 shows the fit distribution in blue, obtained from the subtraction of noise from the signal. The first blue peak around zero is the noise peak, and the second peak is from the first photoelectron. In order to insure that our fit is agreeing with Poisson distribution statistics, the second peak should be less than 10%. If we were triggering photoelectrons 20% of the time instead of 10%, there would be a third peak from the photoelectron overlapped with the second peak. The photoelectrons would be indistinguishable. However, following Poisson statistics allows the distinction of only one photoelectron if its area is less than 10%. As seen in Figure 8, $\Lambda = 4.5\%$, the ratio between the area of signal and the area of noise.

Once we convert the PMT signal to voltage, we can then determine if the PMT is calibrated correctly from its gain. As voltage increases, the PMT gain is expected to increase

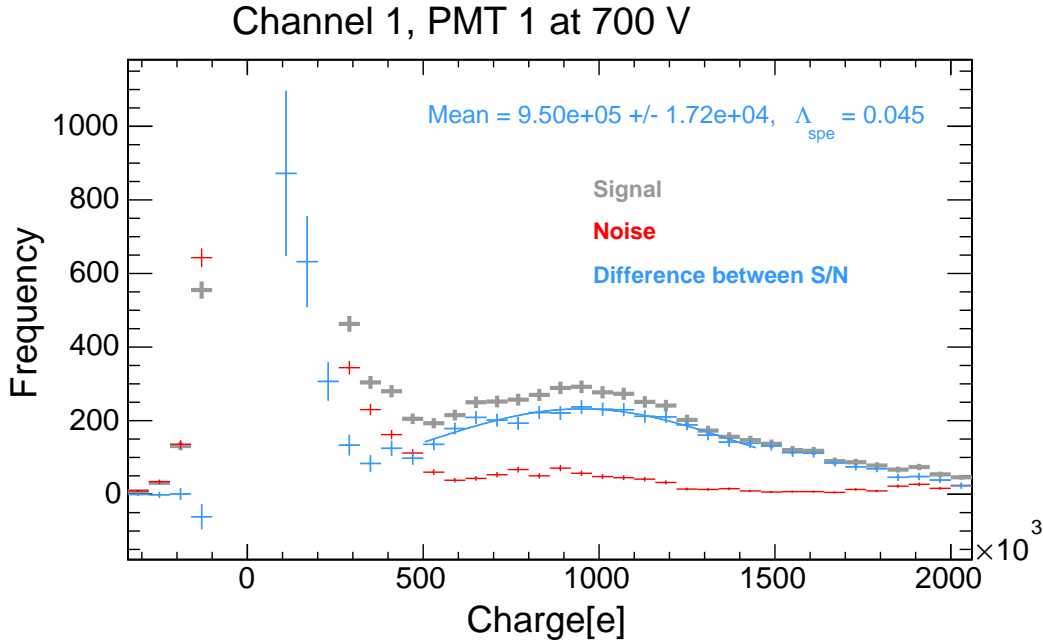


FIG. 7: The first peak is from noise (90% of signal) and the second peak is the first photoelectron (10% of signal)

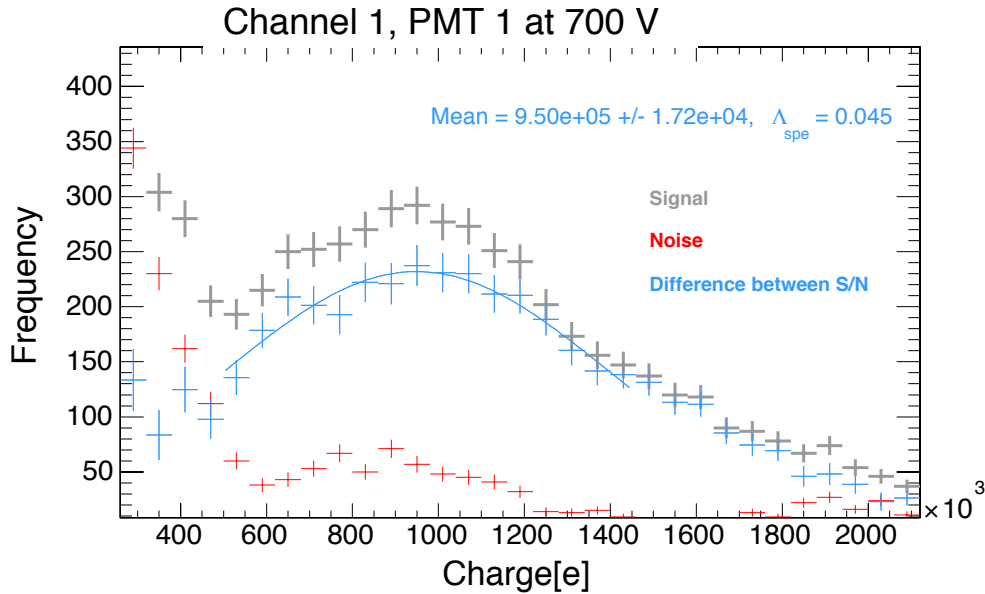


FIG. 8: Second peak scaled, $\Lambda = \text{area of signal} / \text{area of noise} = 4.5\%$. This agrees with Poisson statistics that the first photoelectron is less than 10%.

exponentially, or linearly after taking the logarithm, as seen in Figure 9. Ultimately, the gain needs to be known as a function of voltage on the PMTs. The gain is defined as the number of electrons produced in the photocathode for every photoelectron. The gain is divided by

the quantum efficiency (QE) which is defined as the ratio between the number of electrons produced and the number of incoming photons. The QE for the PMTs in neriX is 35%. Another important factor is the collection efficiency of the PMT which is the probability the photoelectrons will land on the first dynode rather than deviating from their favorable path [5]. After taking these factors into account with the gain, one can calculate the number of incoming photons for a single PMT.

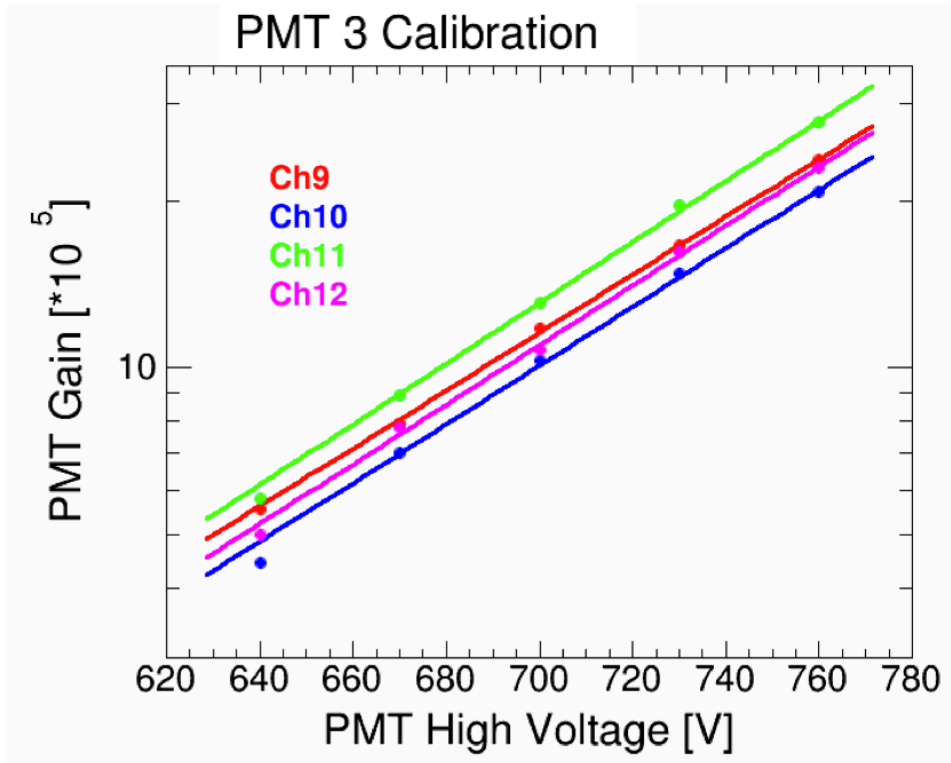


FIG. 9: The PMT gain increases exponentially as voltage increases. Therefore, there should be a linear log fit.[5]

In order to obtain the total number of photons, the scintillation light detection efficiency (LDE) of the LXe detector is taken into account. The LDE is the ratio between the number of photoelectrons for every photon, and depends on the geometry of the detector. After an event, photons will reflect off the sides of the detector, and not all of them will hit the PMTs. After taking all of these factors into account, the total number of photons is calculated and dependent on the type of particle, the recoil energy (E_r), and the electric field (\vec{E}). Then, the scintillation yield is just the ratio between the total number of photons and the recoil

energy. In order to find the ionization yield, there is another gain that is multiplied by the number of photons to give the total number of electrons. This gain arises when electrons pass into the gaseous Xe chamber and collide with more Xe atoms, releasing more electrons. The final ionization yield is the ratio between the total number of electrons and the recoil energy, again depending on type of particle, E_r , and \vec{E} .

It is important to know the scintillation and ionization yields precisely because they allow us to distinguish between nuclear and electronic recoils, as well as calculate the energy scale of the detector. The relative efficiency of nuclear recoils L_{eff} is the parameter used to convert the scintillation signal to nuclear recoil energies [3]

$$L_{eff}(E_{nr}) = \frac{L_{y,nr}(E_{nr})}{L_{y,er}(E_{er})}, \quad (4)$$

In reported LXe WIMP searches, L_{eff} was the largest systematic error at low energies. By varying the scattering angle between the detector and the scintillators, neriX can measure the variation in L_{eff} down to energies of 1keV.

V. PROJECT 2: NEUTRON GENERATOR GEANT4 SIMULATION AND HOLDER DESIGN

A greater flux of neutrons scattering in the LXe detector will allow a faster and more efficient measurement of the scintillation and ionization signals. Increasing the voltage from 40kV to 100kV will produce a stronger neutron beam. However, there are many factors that need to be taken into account with the neutron generator holder when running at 100kV. It is important to calculate the electric field everywhere along the device so that there is not an electrical discharge. In addition, the probability of a neutron scattering in the holder before it reaches the LXe chamber was considered when choosing the dielectric material of the holder.

A. Neutron Generator setup

The neutron generator, as shown in Figure 10, produces neutrons by the ${}^2\text{H}(d,n){}^3\text{He}$ reaction. First, I_{filament} is heated with an electrical current, and deuterium gas is released in the inner volume. The cathode produces another electric current I_{cathode} . As the cathode filament heats up, electrons are extracted to the grid, creating another current I_{grid} between the cathode and grid. The grid is held at positive potential, and a titanium deuteride target is held at negative potential, thus the ionized deuterium gas D_1^+ and D_2^+ accelerate toward the target. When the ions collide with the target, they are either stopped in the target or produce neutrons. The neutrons are mono-energetic, minimizing the spread in neutron energy at a 90 degree angle. It is important to minimize the spread in neutron energy because it is directly proportional to the spread in nuclear recoil energy, as seen in equation 3. [3]

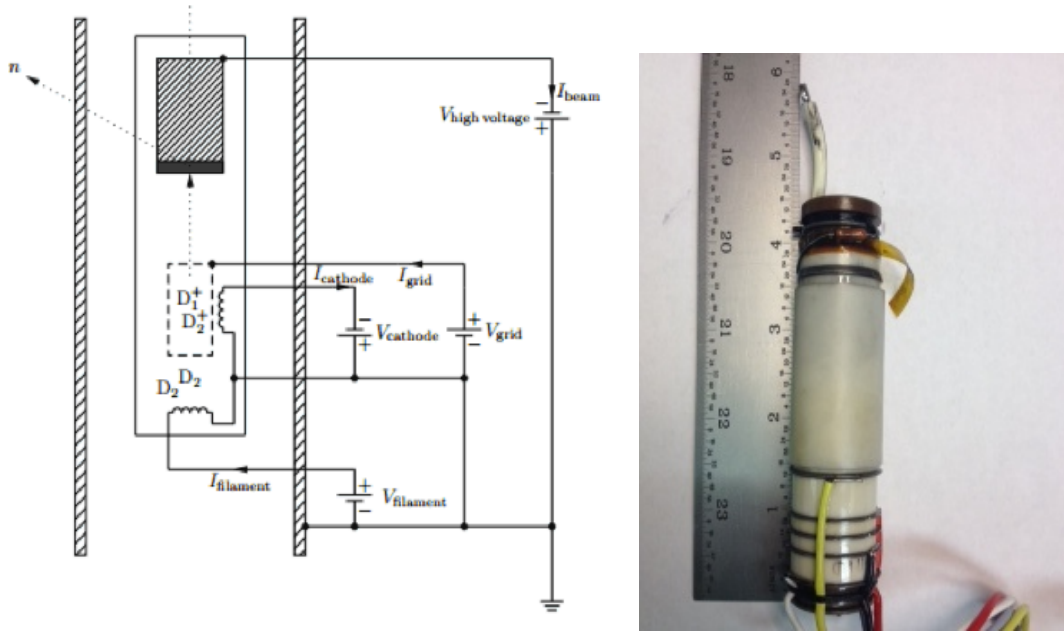


FIG. 10: The neutron generator produces mono-energetic neutrons through the ${}^2\text{H}(d,n){}^3\text{He}$ reaction. [3]

B. Electrical breakdown

At the high voltage cable connection, there needs to be a strong dielectric that will prevent an electrical discharge. The electric field can be modeled as the classic example of a coaxial dielectric cylinder. Following Yung-kuo Lim[6], a cylindrical coaxial capacitor has the capacitance per unit length

$$C = \frac{2\pi\epsilon}{\ln\frac{r}{r_0}}. \quad (5)$$

The outer cylinder is at the higher potential, and we have from $Q = CV$ the charges per unit length on the inner and outer cylinders

$$\lambda_i = -\frac{2\pi\epsilon V}{\ln\frac{r}{r_0}}, \lambda_o = \frac{2\pi\epsilon V}{\ln\frac{r}{r_0}} \quad (6)$$

Using Gauss' law gives

$$E = \frac{\lambda_i}{2\pi\epsilon r}\epsilon_r = -\frac{V}{r\ln\frac{r}{r_0}}\epsilon_r \quad (7)$$

We can model the electric field as a function of the radius as

$$E(r) = \frac{V}{r\ln\frac{r}{r_0}}\epsilon_r \quad (8)$$

where V is the maximum breakdown voltage applied to the wire.

The results of analyzing the Teflon, mineral oil, and air are shown in Figures 11 - 13. Teflon is the only dielectric of the three that does not exceed electrical breakdown at 100kV. Therefore, the hole through the carrier for the HV cable was minimized to insure mostly Teflon will be surrounding the cable. There is also a small amount of oil poured over the carrier to minimize any air gaps. Mineral oil is still a stronger dielectric than air. The dielectric should cover the HV cable at the same length above the cable as the radius of the Teflon tube. In this setup, the radius of the tube is 1.5", so there is 1.5" of dielectric material above the HV cable connection.

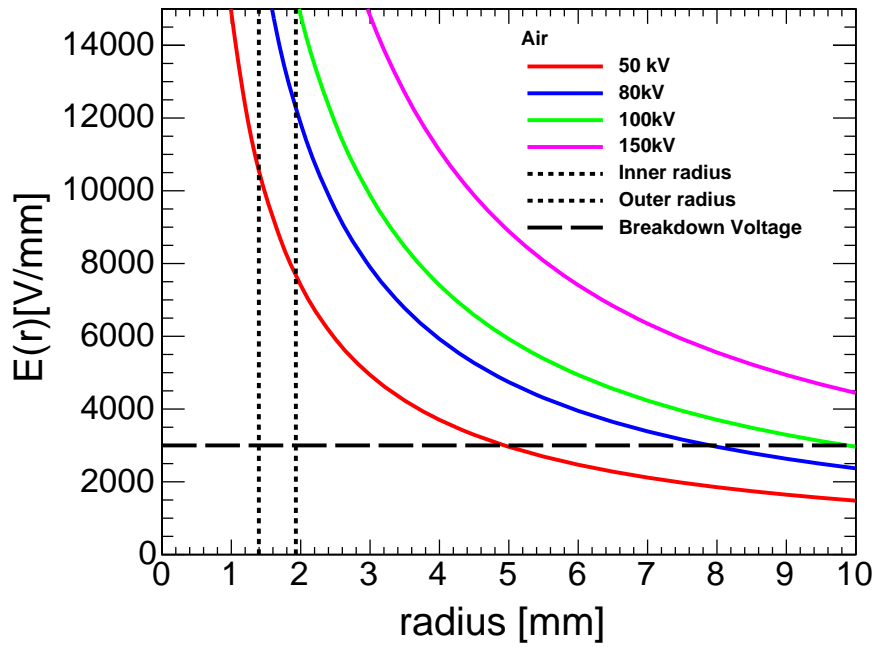


FIG. 11: Electrical breakdown in air shown at the inner and outer radius of the HV cable. The electrical field exceeds maximum electrical breakdown for 100kV at the outer radius.

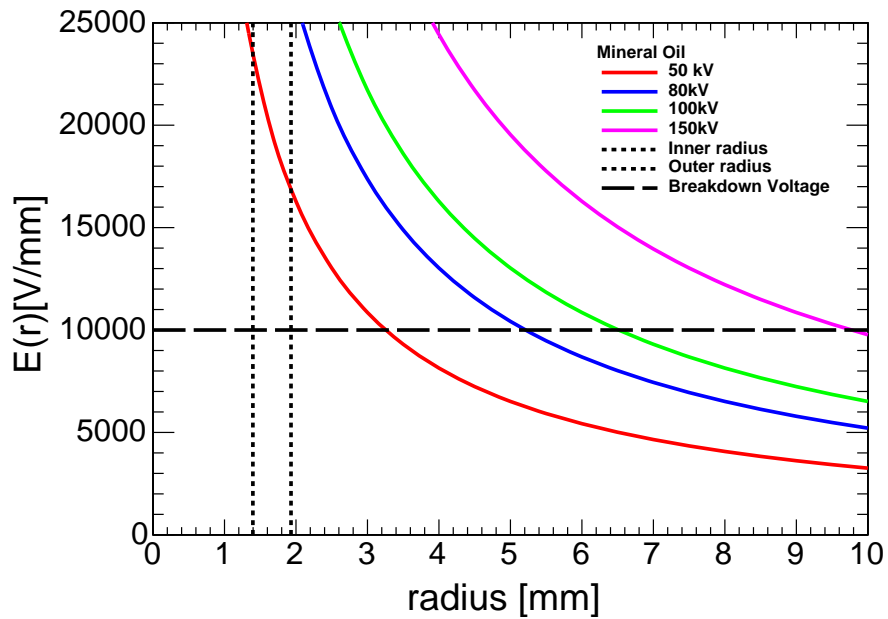


FIG. 12: Electrical breakdown in mineral oil shown at the inner and outer radius of the HV cable. The electrical field exceeds maximum electrical breakdown for 100kV at the outer radius.

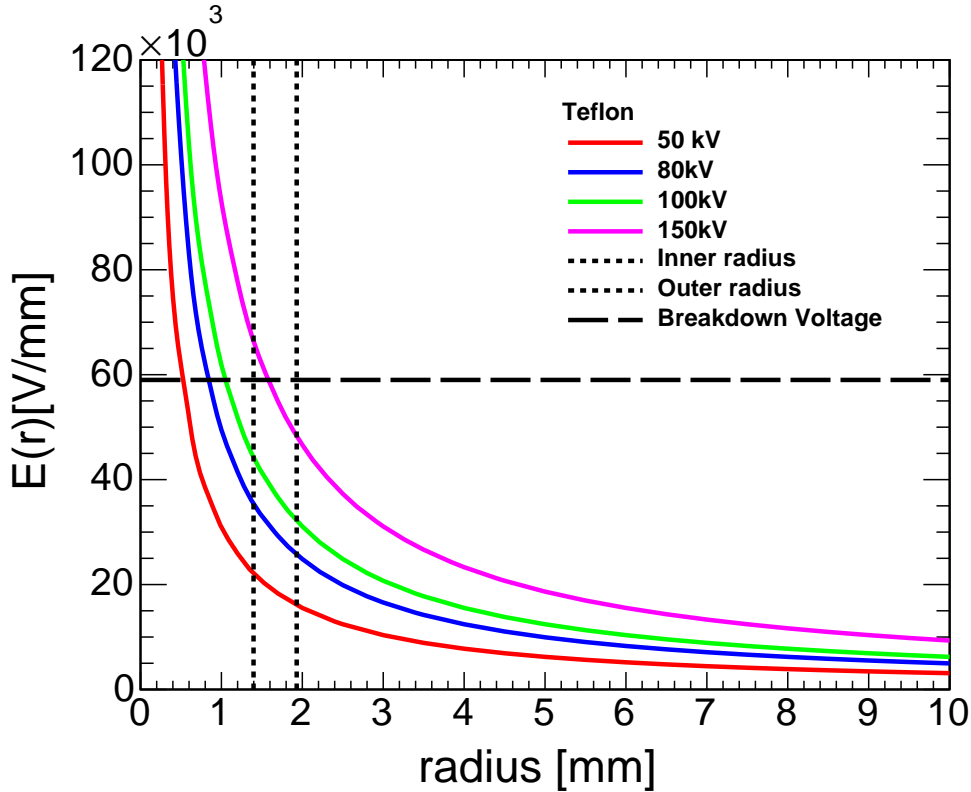


FIG. 13: Electrical breakdown in Teflon shown at the inner and outer radius of the HV cable. The electric field does not exceed maximum electrical breakdown for 100kV at the outer radius. Teflon is the favorable dielectric material to be used in the holder around the HV cable.

C. GEANT4 Monte Carlo Simulation

In order to minimize the amount of neutron scattering within the neutron generator carrier, we need to optimize the ratio between Teflon and mineral oil used for the neutron generator carrier. In order to do so, we performed a Monte Carlo simulation with GEANT4, an image of the carrier is shown in Figure 14. An analysis was performed for three different cuts of the Teflon piece from the center of the tube: 14.8, 25.4, and 32.0mm, as shown in Figures 15 - 17.

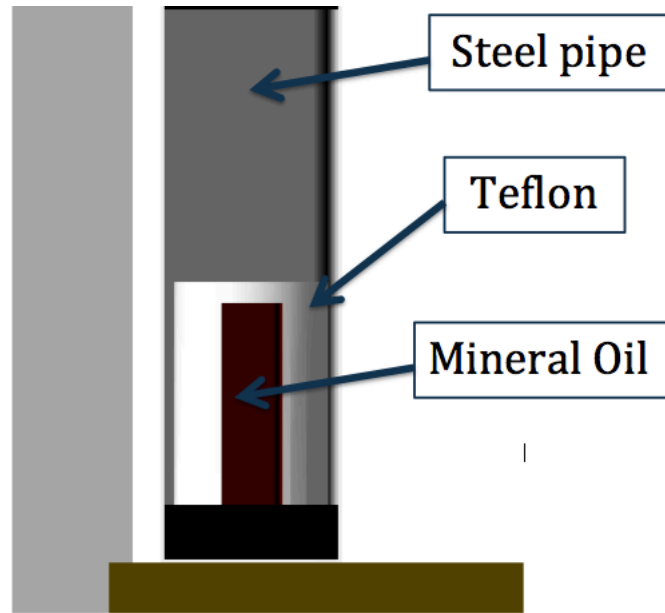


FIG. 14: Image of Teflon holder from GEANT4 simulation. The radius of the hole in the Teflon carrier is the same as the radius of the mineral oil.

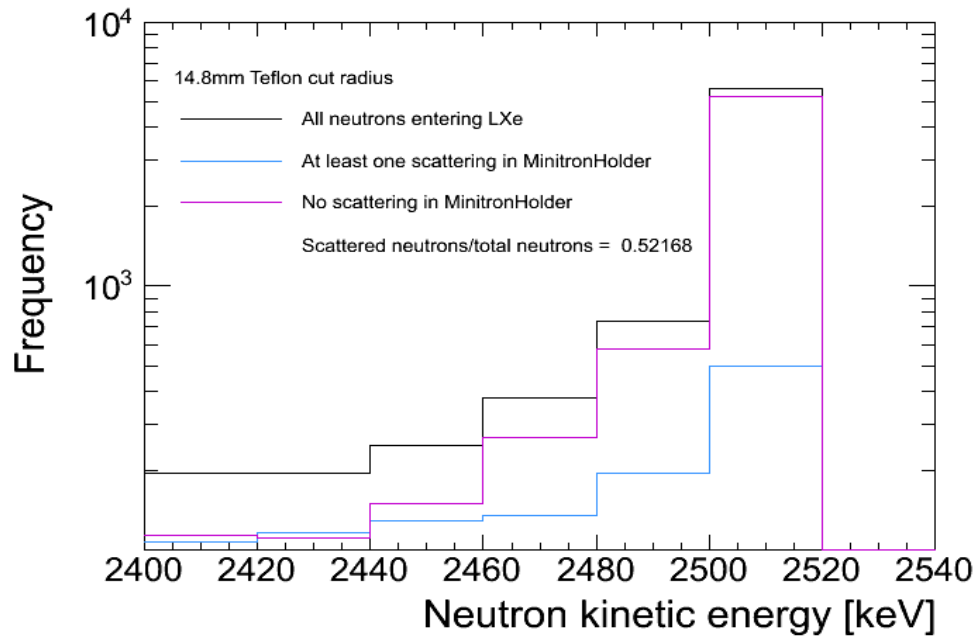


FIG. 15: Model of ratio between Teflon/oil = 1.57. The percentage of neutrons that scatter is 52.2%

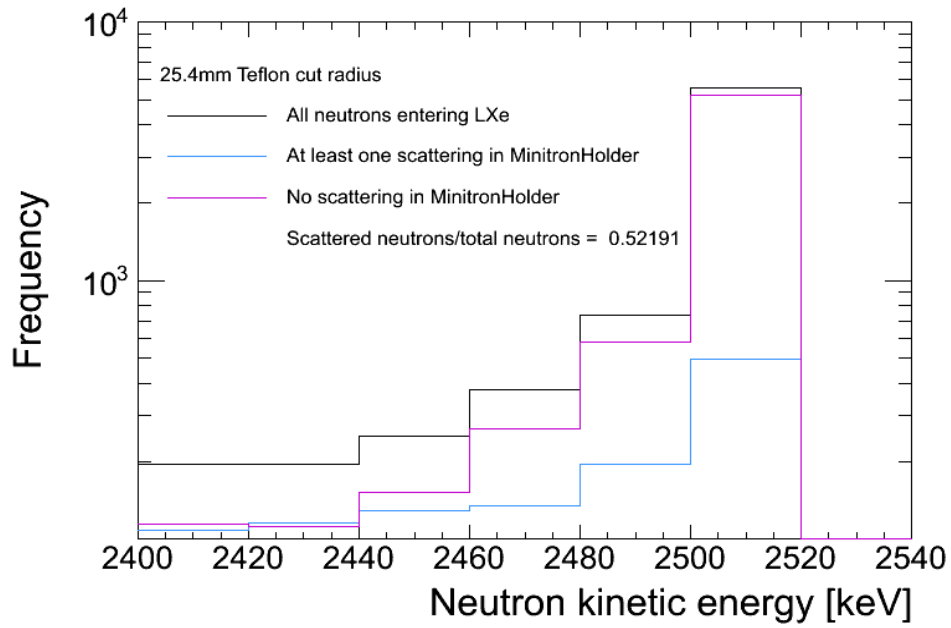


FIG. 16: Model of ratio between Teflon/oil = 0.50. The percentage of neutrons that scatter is 52.2%

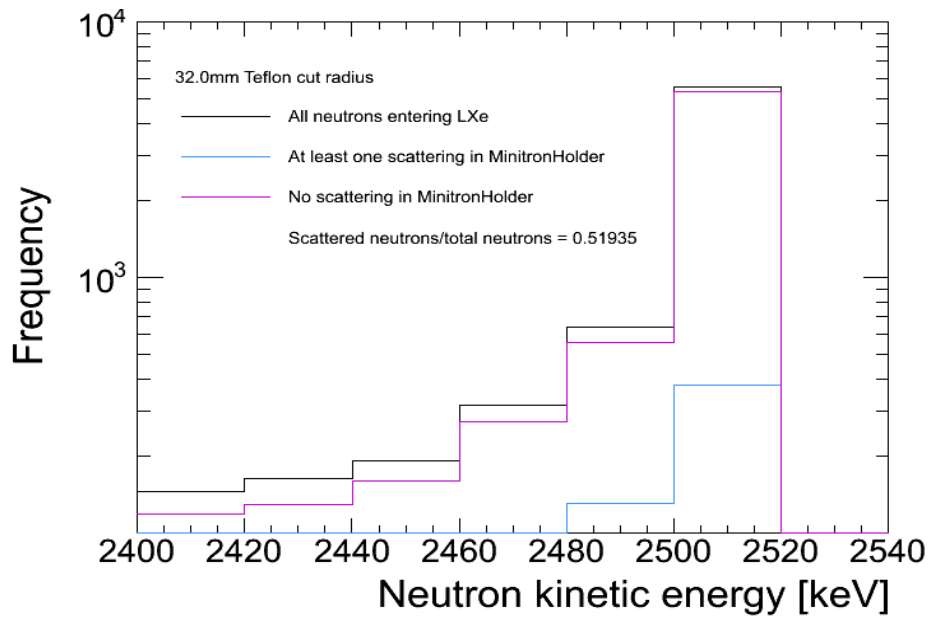


FIG. 17: Model of ratio between Teflon/oil = 0.19. The percentage of neutrons that scatter is 52.0%

As a result of the Monte Carlo simulation, the the largest cut in Teflon produced the smallest amount of scattering as shown in Figure 18. However, the entire carrier is 38.1mm so a Teflon cut of 32.0mm leaves 32.0mm of mineral oil and only 6.1mm of Teflon. This is not a practical design because the carrier would not hold the neutron generator in a fixed position. In addition, the amount in variation of neutron scattering is negligible, about $\pm 0.4\%$. Conclusively, the final carrier design maximizes the use of Teflon to provide low scattering and keep the neutron generator stable. Keeping the neutron generator immobile is important when detecting the scattered neutrons at fixed angles with the scintillators.

Teflon cut (mm)	Teflon/Oil	Scattered/Total neutrons
14.8	1.57	0.522
25.4	0.50	0.522
32.0	0.19	0.520

FIG. 18: Percentage of neutron scattering according to the ratio between Teflon/oil. The difference in the ratios is negligible in terms of neutron scattering.

Using SolidWorks, I designed the final model for the neutron generator carrier as shown in Figure 19 and 20. The outside steel tube provides stability and a steel tee pipe guides the neutron generators' cables. There is also an extra bottom piece of acrylic that is used to provide a gap in which the bottom wires of the neutron generator can be easily guided. Three acrylic stands are used to connect the extra bottom part to the bottom of the carrier. The carrier shown in Figure 20 is placed inside the tube with a very tight fit in order to maximum the amount of Teflon. The bottom and top parts interlock and minimize the hole in which the generator fits inside. This maximizes the amount of teflon used as well.

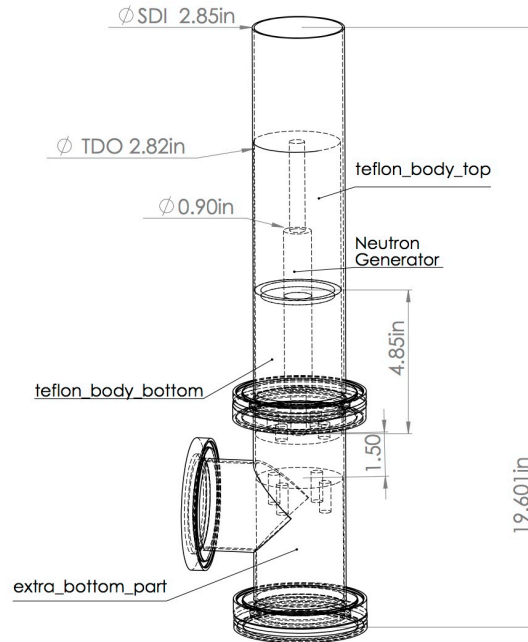


FIG. 19: SolidWorks design for neutron generator carrier consisting of a surrounding steel pipe, two teflon carrier pieces, and an acrylic stand.

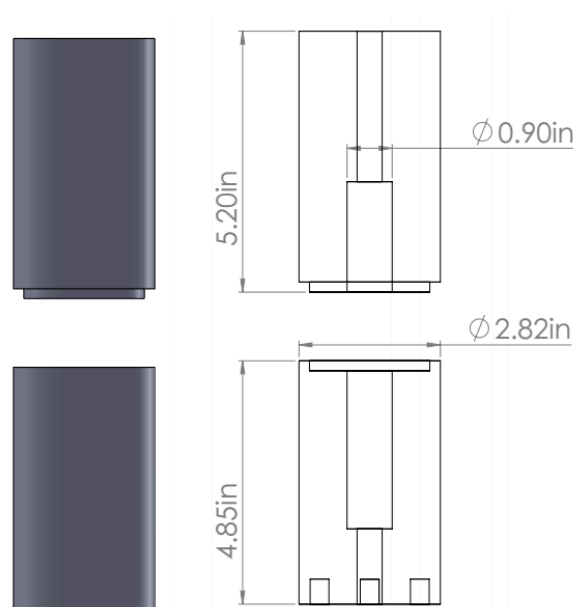


FIG. 20: Top and bottom part of the Teflon carrier. Once the neutron generator is placed inside, the carrier is placed in the steel pipe and filled with mineral oil.

VI. CONCLUSION

The PMT calibrations need to be made on a continuous basis to insure neriX is precisely detecting the scintillation and ionization signals. By graphing the PMT gain as a function

of voltage, it is easiest to determine the voltage at which to operate the PMT to achieve the desired gain. In addition, the improved neutron generator carrier design will allow neriX to operate at over 100kV compared to the previous 40kV. The carrier firmly secures the neutron generator, reducing the experimental error of the neutron generator position changing over time. The modified carrier also minimizes the amount of neutron scattering within the carrier so that the greatest flux of neutrons is hitting the LXe detector.

VII. ACKNOWLEDGEMENTS

I would like to acknowledge Elena Aprile, Antonio Melgarejo, Luke Goetzke, Marc Weber, Matthew Anthony, and the XENON collaboration at Nevis for their support and guidance throughout the REU summer program. I would also like to thank Columbia University and the NSF for their generous funding.

-
- [1] Zwicky, F., *Spectral Displacement of Extra Galactic Nebulae*, (Helv. Phys. Acta, 6). 110-127 (1933): 15
 - [2] Clowe, D. et al., *A Direct Empirical Proof of the Existence of Dark Matter*, *Astrophys. J. Lett.*, 648 (2006), L109.
 - [3] Plante, G., *The XENON100 Dark Matter Experiment: Design, Construction, Calibration and 2010 Search Results with Improved Measurement of the Scintillation Response of Liquid Xenon to Low Energy Nuclear Recoils*, Ph.D. thesis, Columbia University, NY, 2012.
 - [4] Baudis, L., *Direct dark matter detection: the next decade*, (2012), arXiv: 1211.7222v1.
 - [5] Melgarejo, A., *Liquid Argon Detectors for Rare Event Searches*, Ph.D. thesis, University of Granada, Granada, 2008.
 - [6] Lim, Y., *Problems and Solutions on Electromagnetism*, Singapore: World Scientific 1990.